Entangled Cross-Linked Fibres for an Application as Core Material for Sandwich Structures - Part II: Analytical Model

L. Mezeix [1,2] · D. Poquillon [1] · C. Bouvet [2]

Abstract Entangled cross-linked carbon, aramid and glass fibres were recently produced by epoxy spraying for an application as core material for sandwich panel. The Young's moduli in compression and tension have been previously measured and briefly summarized in this paper. To optimize the core structure, modelling of these properties has been achieved in the present paper. The cross-link fibres have a random orientation and the stiffness of the epoxy joint is modelled by a torsion spring. A parallel model is chosen for homogenisation. It was found that the experimentally estimated stiffness of these materials fits fairly well with the modelled ones.

Keywords Entangled fibres · Mechanical properties · Modelling · Sandwich structure · Core material

1 Introduction

Sandwich structures are commonly used in aerospace, naval construction, and transport structures, since they offer a great stiffness over weight ratio. The purpose of the core is to maintain the distance between the skins and to resist the shear deformation. A variation of the core, the thickness and the material of the face sheet of the sandwich structures, makes it possible to obtain various properties and the desired performance [1–4]. Typical core configurations include different foams, honeycomb or lattice core material.

Entangled cross-linked fibres present a strong interest in highly porous metals for a wide range of applications [5–11]. They present a relatively low density, a high porosity and a simplicity of production thanks to its cost-effective routes with considerable versatility as far as type of fibres and architecture are concerned. Entangled cross-linked fibres can be made by assembling a set of metallic fibres and bonding them together by different processes such as

✉ C. Bouvet
christophe.bouvet@isae.fr

[1] Université de Toulouse, CIRIMAT, INPT-ENSIACET, 4 allée Emile Monso, BP 44362, 31432 Toulouse Cedex 4, France

[2] Université de Toulouse, ICA, ISAE, 10 avenue Edouard Belin, BP 54032, 31055 Toulouse, France

welding, brazing, sintering or adhesive bonding [9, 12, 13]. Recently, a new type of entangled cross-linked fibres was developed based on entangled carbon, aramid and glass fibres bonded by epoxy vaporization [5, 14–16]. This material has the potential to exhibit an attractive combination of properties for sandwich application, such as an open porosity, multifunctional properties or the possibility to obtain complex shapes [5].

Many studies have been carried out on the mechanical characteristics of bonded fibre arrays [12, 14, 17–20]. Gibson and Ashby works concerned with modelling of open cell foams. [17] can be applied to entangled cross-linked fibres. Markaki and Clyne developed a simple analytical model based on the bending of individual fibres, in order to predict the mechanical response of metallic bonded fibres when subjected to either mechanical or magnetic forces [12]. However, perfect bonding is modelled between fibres and therefore the stiffness of the joint is not considered.

Therefore, in the present paper an analytical model was developed to predict the initial stiffness of entangled cross-linked fibres bonded by epoxy spraying. The stiffness of the epoxy joints is represented by a torsion spring and its value is determined by a FE model where the geometry is obtained by SEM observations. The results were then examined with respect to the experimental Young moduli identified in Part I of the current work.

2 Materials

Different types of fibres, i.e. carbon, glass and aramid, were used as entangled cross-linked fibres [5]. In this study we used a constant density of 150 kg/m^3 for the fibres and 30 kg/m^3 for the vaporized resin. As the density was not the same for all the fibres, the fibres volume fraction, f, of the tests materials was different (Table 1). Compression and tensile tested were performed and the Young's moduli were always measured during unloading. According to the experiments, the mechanical behaviour of the entangled cross-linked fibres can be summarized as follows [5]: Firstly, carbon fibres present a higher stiffness than glass and aramid fibres for the same fibres density (Table 2). This is mainly due to the shortest distance, L, between epoxy joints (Table 1). Secondly, two different epoxy resins were used to study their influence on the stiffness of the material and no difference was noted (Table 2). It was also observed that the stiffness of the epoxy joints is smaller with the weakest resin but on the other hand, the distance between joints is shorter on the material made with this resin. Moreover, Young modulus experimentally measured was found higher in tension than in compression. This is probably due to the additional stiffness of the vertical fibres (Table 2).

Table 1 Properties and volume fraction of used fibres: $^{(1)}$ in compression and $^{(2)}$ in tension [5]. L is the average of the values determined by SEM observations

Fibres	D [μm]	E_f [GPa]	E_fI [N.mm^2]	f %	L [μm]	Resin reference
Carbon fibres	7	240	2.8×10^{-5}	8.5	100	SR8100
					120	SR1710
Aramid fibres	12.5	$36^{(1)}/120^{(2)}$	4.3×10^{-5}	10.7	180	SR1710
Glass fibres	12	73	7.4×10^{-5}	5.9	200	SR1710

Table 2 Experimental Young modulus in compression and tension [5]

Fibres	E (compression)	E (tension)	Resin reference
Carbon fibres	5	17.5	SR1710
	5	–	SR8100
Aramid fibres	3.1	6.5	SR1710
Glass fibres	1.7	4.4	SR1710

3 Analytical Model

3.1 Deflection of Individual Fibre

Using a homogenization approach, the model integrates fibres behaviour to get the macroscopic behaviour of the material. All fibres are supposed to have the same displacement as detailed in Fig. 1a (Voigt approach).

The model consists of individually oriented fibres by an angle θ, considered as a beam of length, L (Fig. 1b). This length represents the average distance between two epoxy joints. At each extremity of the beam, a torsion spring represents the stiffness of the epoxy joints. The beam is subjected to an imposed vertical displacement (Δz). It can be decomposed in a bending part (Δf) and in a compression part (ΔL). The force generated by the compression part has no bearing on the stiffness calculation. Due to the high ratio distance, L, between epoxy joints over fibres diameter, D, the fibres may buckle.

The displacement due to flexion (Δf) creates a bending force (w_f), whose horizontal part will randomly cancel the horizontal parts of other fibres. The vertical part, $W_{bending}$, generates the compression force. The mathematical relationship of this compression force, $W_{bending}$ is (Eq. (1)):

$$W_{bending} = \frac{12E_f I \Delta z \sin^2\theta}{JL^3} \tag{1}$$

$$\text{With} \qquad J = 1 + \frac{6E_f I}{KL} \tag{2}$$

Where E_f is the fibres Young modulus, K is the stiffness of the spring representing the stiffness of the epoxy joint and I is the moment of inertia of the cylindrical fibre section in bending (Eq. (3)):

$$I = \frac{\pi D^4}{64} \tag{3}$$

3.2 Determination of Epoxy Joint Stiffness

The stiffness of the epoxy joint, K, between two fibres is obtained in two steps. Firstly, the epoxy junction is modelled by a Finite Element model, where the geometry is drawn based on SEM observations (Fig. 2). The geometry of the junction depends on the type of fibres. The fibres and epoxy material are considered as homogeneous and their behaviours as elastic linear. Under a torsion load, F, the displacement, δ_f, of the fibres is obtained (Fig. 2).

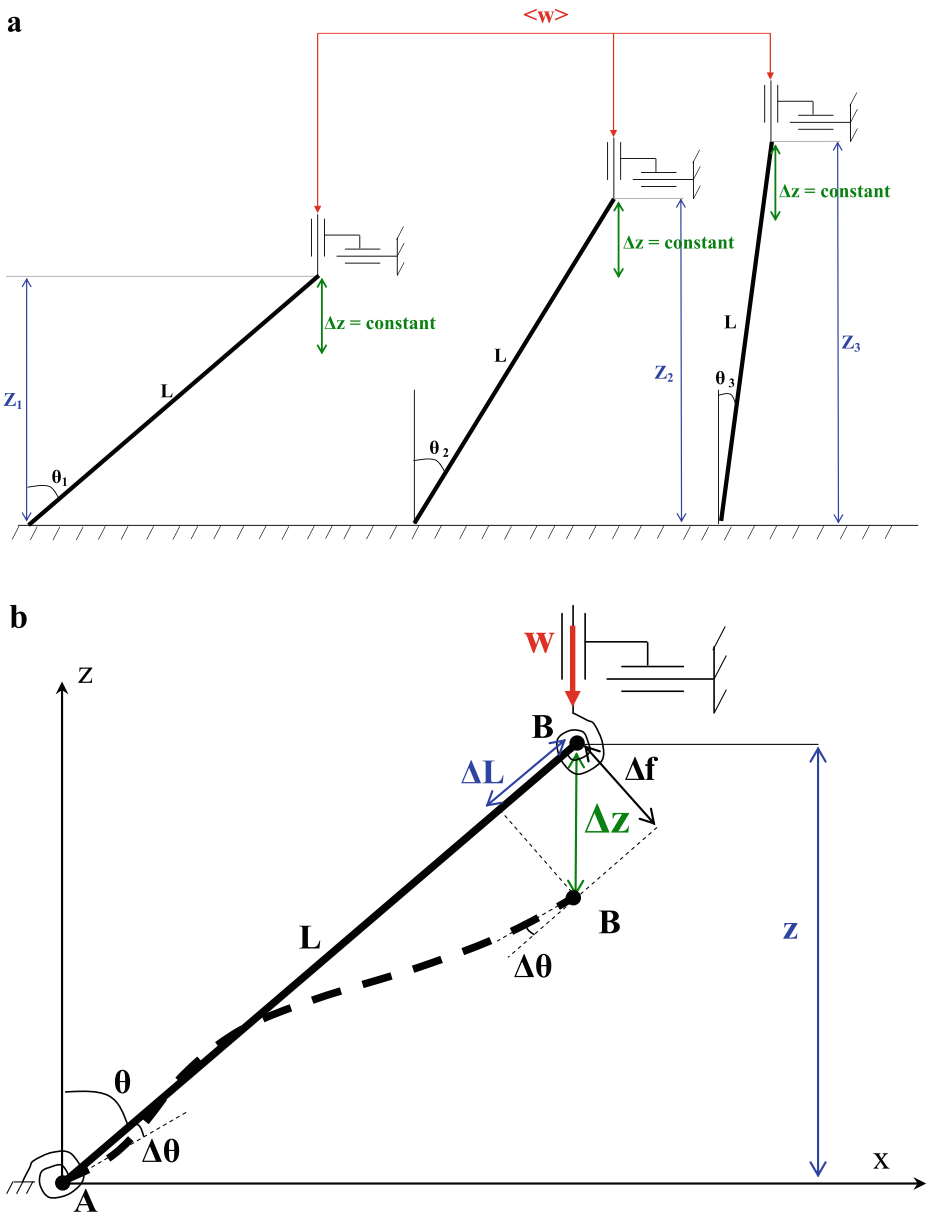

Fig. 1 Schematic representation of (**a**) the parallel architecture of the fibres and (**b**) the beam under the influence of a vertical displacement, Δz

Secondly, thanks to the relation between the torsion load and the displacement obtained by the FE model, the torsion spring stiffness, K, is determined by an analytical model (Fig. 3) from the small strain (Eq. (4)):

$$K = \frac{FL^2}{\delta_f} - \frac{3EI}{L} \tag{4}$$

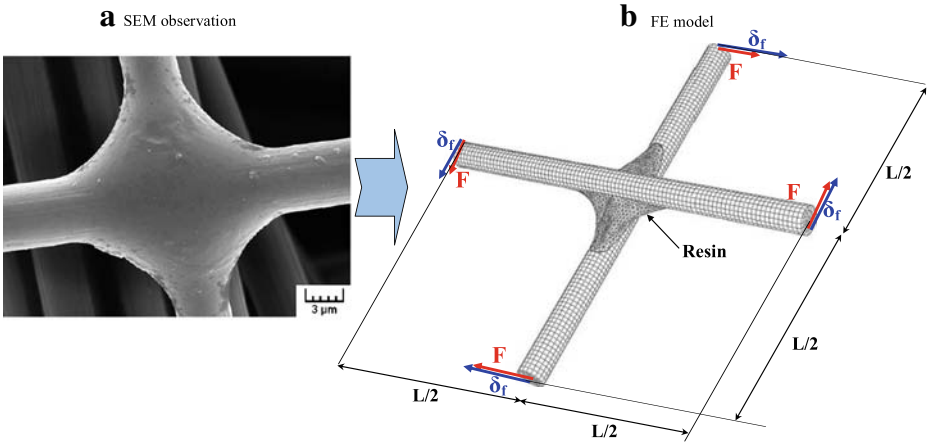

Fig. 2 (**a**) Typical joint observed by SEM and (**b**) junction modelled by FE

The values of the stiffness are presented in the Table 3. Due to the small fibres diameter, the spring stiffness is lower in the case of carbon fibres.

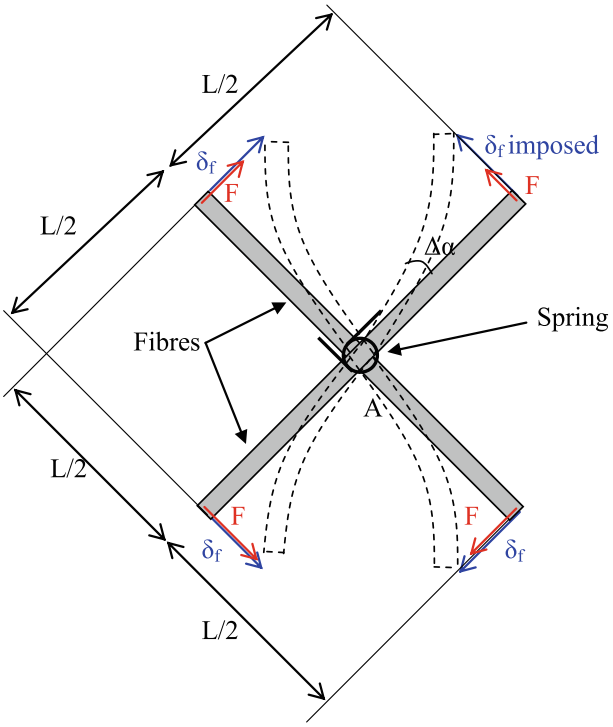

Fig. 3 (a) Schematic representation of the analytical model

Table 3 Stiffness of torsion spring obtained by the model

	Carbon SR1710(SR8100)	Glass SR1710	Aramid SR1710
K [10^{-4} N.mm]	23.6(12.6)	170	101

3.3 Elastic Deformation of Entangled Cross-Linked Fibres Under Compression

The overall applied stress is related to the axial load on individual fibre segments, by (Eq. (5)):

$$\sigma = N\left\langle W_{bending}\right\rangle \tag{5}$$

Where N is the number of fibre segments per unit sectional area, and the value of N is given for 3D randomly oriented fibres by (Eq. (6)) [21]:

$$N = \frac{2f}{\pi D^2} \tag{6}$$

If it is assumed that interactions between neighbouring fibres have limited effects on the average force resulting from the vertical displacement, so <$W_{bending}$>can be obtained by simple integration, taking into account the fact that an isotropic fibre orientation distribution exhibits a sinθ probability [12]:

$$\left\langle W_{bending}\right\rangle = \frac{\int_0^{\pi/2} W_{bending}\sin\theta d\theta}{\int_0^{\pi/2} \sin\theta d\theta} \tag{7}$$

Using a Voigt homogenization approach (Fig. 2a), the macroscopic strain is given by (Eq. (8)):

$$\varepsilon = \frac{\Delta z}{\langle z\rangle} = \Delta z.\frac{\int_0^{\pi/2} \sin\theta d\theta}{\int_0^{\pi/2} L\cos\theta\sin\theta d\theta} \tag{8}$$

Where <z> is the average fibres height by taking the orientation probability into account. The Young's modulus E (=σ/ε) is therefore given by (Eq. (9)):

$$E = \frac{E_f f}{8J\left(\frac{L}{D}\right)^2} \tag{9}$$

3.4 Elastic Deformation of Entangled Cross-Linked Fibres Under Tension

Irrespective of the nature of fibres used, entangled cross-linked fibres present higher stiffness in tension than in compression due to the additional rigidity of the quasi vertical fibres, while

in compression they buckle quickly [5]. Therefore, analytical model needs to be adapted to consider this additional rigidity.

The beam is always subjected to an imposed vertical displacement (Δz). It can be divided into a bending part (Δf) and a tension part (ΔL), but here the force generated by the tension part is taken into consideration for the computation of the stiffness. But all the fibres should not work in tension; only the quasi vertical fibres should really load in tension, while in compression they buckle quickly. The quasi-vertical fibres should be the fibres between the vertical and those oriented by a low angle θ_0. As the tension load is also considered, the overall applied stress is related to the tension and bending loads on individual fibre segments by (Eq. (10)):

$$\sigma = N_{bending}\langle W_{bending}\rangle + N_{tension}\langle W_{tension}\rangle \tag{10}$$

Where $N_{bending}$ and $\langle W_{bending}\rangle$ are given by the Eq. (1) and Eq. (5), and $W_{tension}$ is obtained by the behaviour of a beam in tension (Fig. 4) (Eq. (11)):

$$W_{tension} = \frac{E_f \pi D^2 \Delta z \cos^2\theta}{4L} \tag{11}$$

As for the bending part, $\langle W_{tension}\rangle$ can be obtained by a simple integration, taking into account the fact that an isotropic fibre orientation distribution exhibits a sinθ probability. But for the tension, only the fibres between the vertical and an angle of $\theta=\theta_0$ is considered. So the overall stress due to the tension load is (Eq. (12)):

$$N_{tension}\langle W_{tension}\rangle = \frac{\int_0^{\theta_0} \frac{E_f \pi D^2 \Delta z}{4L}\cos^2\theta\sin\theta d\theta}{\int_0^{\pi/2}\sin\theta d\theta} \tag{12}$$

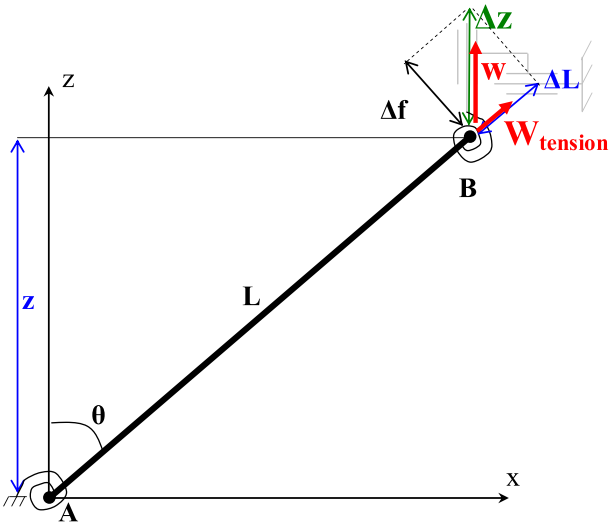

Fig. 4 Schematic representation of the beam under the influence of a vertical displacement in tension

Where the number of fibre segments per unit sectional area is in tension (Eq. (13)):

$$N_{tension} = \frac{\int_0^{\theta_0} \frac{4f}{\pi D^2} \cos\theta \sin\theta d\theta}{\int_0^{\pi/2} \sin\theta d\theta} \tag{13}$$

4 Results and Discussions

4.1 Elastic Deformation of Entangled Cross-Linked Fibres Under Compression

Results obtained by Eq. (9) can be compared with the expression given by Gibson and Ashby [17] for open cell foam. These author's hypotheses are also based on beam deflections (3-point bending under a normal load), but the geometry is more constrained (Eq. (14)):

$$E_{GA} = \frac{3\pi E_f}{4\left(\frac{L}{D}\right)^4} \tag{14}$$

Equation (9) can be also compared with the work of Markaki and Clyne [12] for metallic fibres arrays. In this article, the calculations are also based on clamped cantilever beam deflections, but Reuss homogenization is used. Then these authors predicted (Eq. (15)):

$$E_{MC} = \frac{9E_f f}{32\left(\frac{L}{D}\right)^2} \tag{15}$$

Figure 5 compares the results obtained by the different models (Eqs. (9), (14) and (15)). For all the material tested, the proposed model predicts the Young modulus correctly.

4.2 Effect of the Junction Stiffness

Predicted Young's moduli (Eq. (9)) are elaborated in Fig. 6 as a function of the spring stiffness, that represents the epoxy joint stiffness. Figure 6 also details the experimental initial Young's moduli for the different fibres materials [5]. For all configurations tested, the stiffness of the material increases with the value of the spring stiffness (1). The value of the stiffness tends towards the experimentally obtained value when the stiffness of the junction is the value predicted using FE model of the junction. Moreover it would be possible to increase significantly the material stiffness, especially with carbon fibres, by using a higher rigidity resin. But a modification of the resin causes also a change in viscosity and therefore the distance between junctions. Moreover the largest effect of the spring stiffness on the carbon fibres stiffness is due to the smallest diameter, D, of this type of fibre (size of the junction). Furthermore, a smaller diameter induces a smaller distance between junctions.

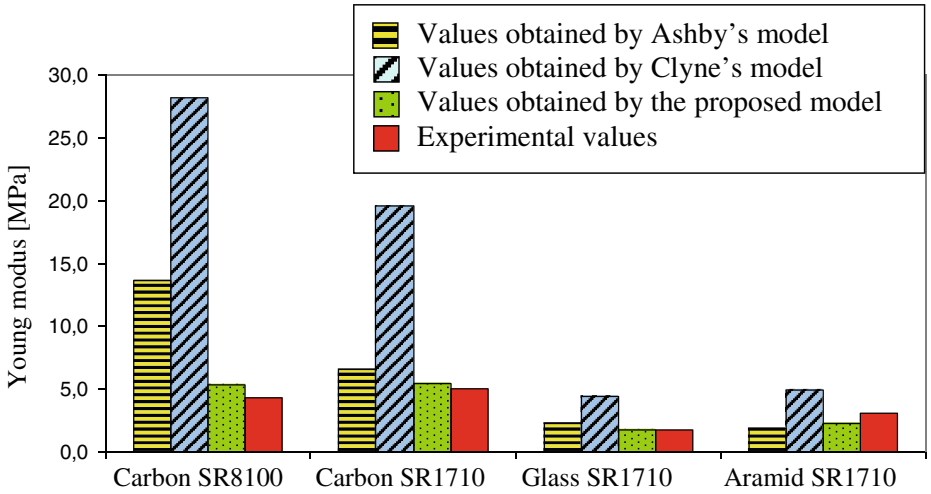

Fig. 5 Comparison between the Young modulus obtained by the proposed model (Eq. (9)) and models of Clyne (Eq. (14) [12]) and Ashby (Eq. (15) [17])

The effect of the spring stiffness for different distances between joints is now studied (Fig. 7). Firstly, if the distance, L, is short, then the stiffness of the material is higher. Secondly, for a short distance between joints, the value of the spring stiffness must be high, in order to raise the asymptote (1). While for a long distance between joints, a spring with a low stiffness is required (2). The displacement of the fibres in this case is mainly due to the bending displacement of the beam. When this distance decreases, the stiffness is mainly due to the spring stiffness, which shows that the spring has a greater influence.

Even without any available experimental data, it is interesting to study the Young's modulus for different fibres diameters (Fig. 8). For a small diameter, the size of the junction does not need to be large to bond fibres so the stiffness value of the junction is quickly considered as infinity. For fibres with a small diameter, the displacement of the fibres is mainly due to the bending of the beam. For larger diameters, the junction is larger, so its stiffness increases. A greater fibre diameter results in an increased size and rigidity of the epoxy junction. However, as the diameter of the fibre increases, its bending stiffness (EI) also increases with the stiffness of the epoxy junctions.

4.3 Effect of the Distance Between Junctions

The distance between joints is one of the main parameters related to stiffness. This distance depends on the volume fraction of the fibres, f, and on the quantity of the vaporized resin. Therefore, effect of this distance, L, can be studied independently from others parameters (Fig. 9). As discussed previously, all the materials are made with a constant fibres density (150 kg/m^3), so the volume fraction, f, of the samples differs with the fibres (Table 1). As the average distance between fibre contacts (no cross-linked), $L_{contact}$, is related to the diameter and the volume fraction of the fibres, we can determine the shortest theoretical distance between junctions for a 3D random fibres material (Eq. (16)) [22–24]:

$$L_{contact} = \frac{D}{2f} \tag{16}$$

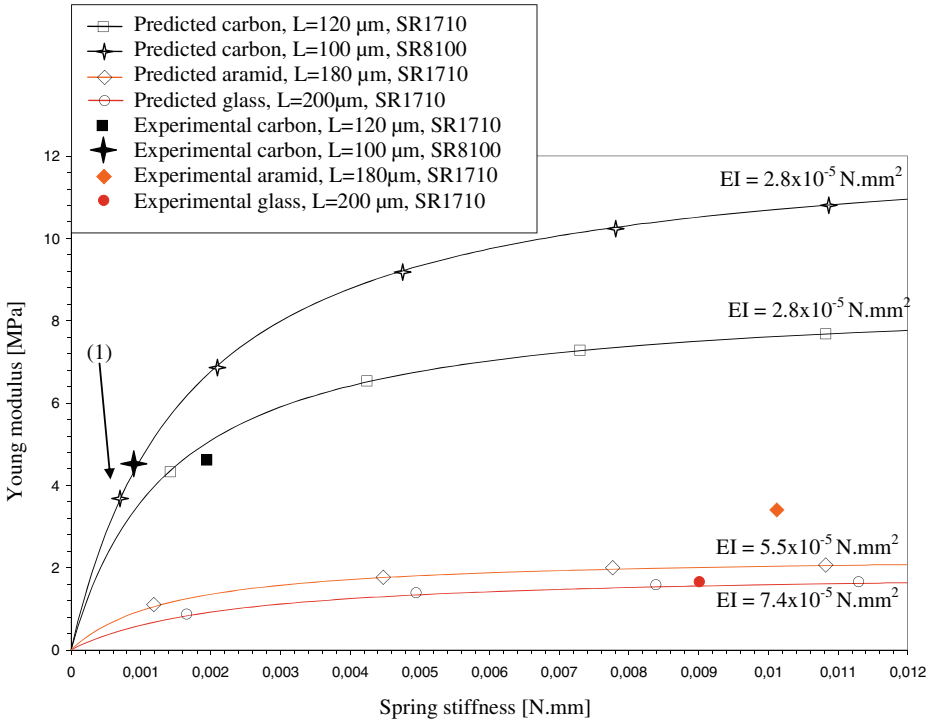

Fig. 6 Evolution of the Young modulus of the material as a function of the spring stiffness

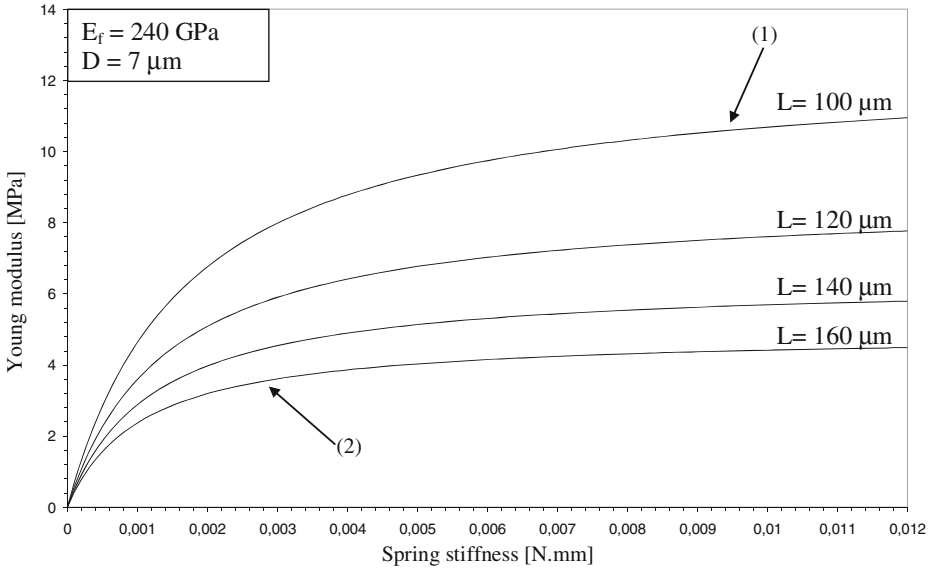

Fig. 7 Evolution of the Young modulus of the entangled cross-linked carbon fibres as a function of the spring stiffness for different values of the distance between junctions

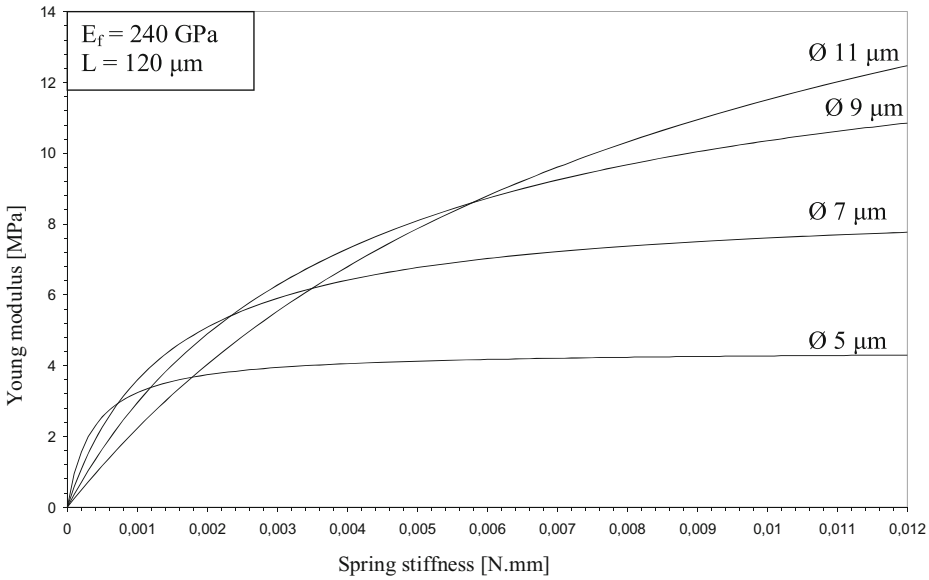

Fig. 8 Evolution of the Young modulus of the entangled cross-linked carbon fibres as a function of the spring stiffness for different values of the fibre diameter

In the case of our samples, the theoretical distance between fibre contact, in case of carbon, amid and glass fibres is respectively 41, 58 and 100 µm. It is important to note that this model was developed for idealized rigid fibres, which is not the case in our present study. Moreover, due to our fabrication process, each fibres contact may not be bonded by epoxy. So the distance obtained using Eq. (16) is an approximation of the lowest distance we can obtain. Thus the predicted Young modulus could be significantly larger than the experimental value, as shown on Fig. 9.

4.4 Elastic Deformation of Entangled Cross-Linked Fibres Under Tension

A sequential approach is achieved to determine θ_0. Indeed, as no experimental data can be used to determine θ_0, therefore it will be determined using the model (Eq. (9)). θ_0 will be that cut off value for which the experimental Young modulus of the entangled cross-linked carbon fibres equals the predicted one. These carbon fibres were chosen because more observations were made on them to measure the distance, L, between junctions. The value of $\theta_0 \approx 15°$ leads to the appropriate stiffness. As the fibre length is very large compared to the distance between junctions, the fibres length does not have any influence. So the calculation of the Young's modulus in tension can be realised for the others fibres using this θ_0 value. We can note that the stiffness obtained is close to the measured modulus (Fig. 10). Therefore, the identification of the angle (θ_0) seems appropriate.

In order to model tension behaviour, the assumption to take only the fibres between the stress direction and an angle θ_0 of 15°, seems to be pertinent. However, additional experiments need to be carried out with others types of fibres to confirm this result. In addition, the effect of fibres length on the angle θ_0 also needs to be studied.

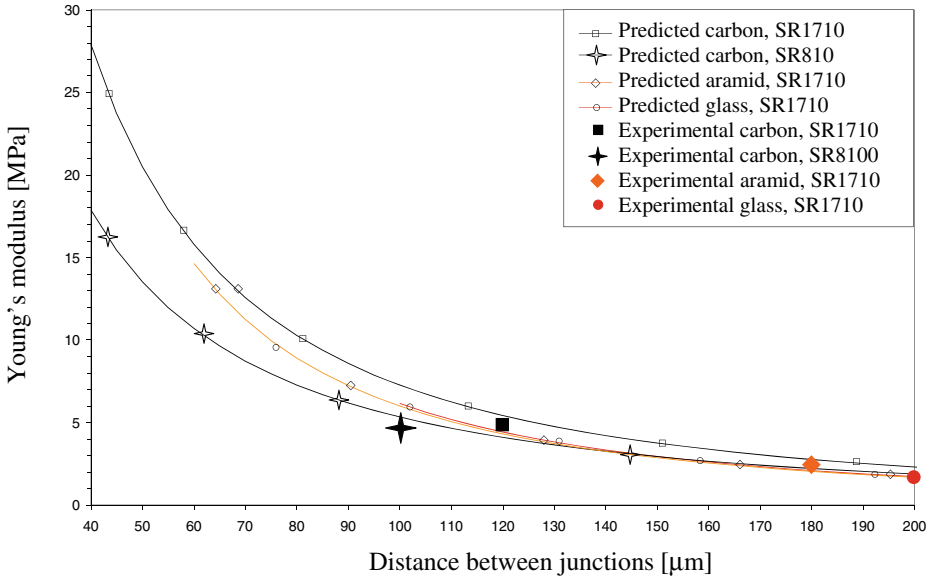

Fig. 9 Young's modulus predicted by the model (Eq. (8)) as a function of the distance between junctions

5 Conclusion

This paper relates to entangled cross-linked fibres bonded by epoxy vaporization. A simple analytical model is developed to predict the response of these entangled cross-linked fibres under compression and tension load. The following conclusions can be drawn:

- From an analytical model based on the bending of fibres, expressions of Young modulus in compression are obtained. The form of the prediction is similar to that of a previously developed expression by Markaki and Clyne [12], based on the bending beam. However, in the model developed in this study, a Voigt approach is used and the epoxy joints

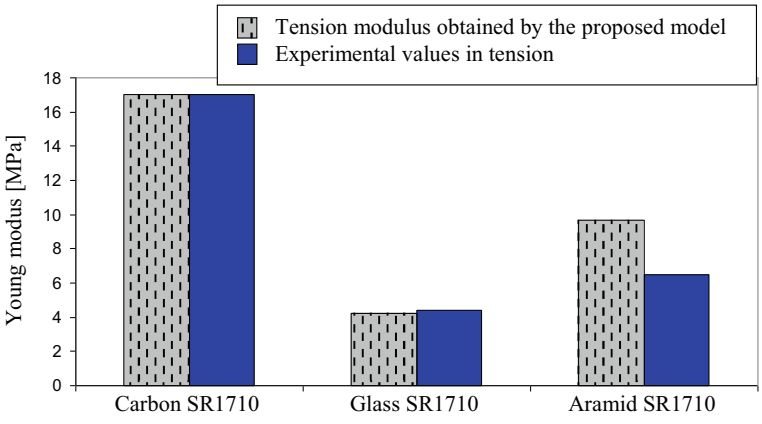

Fig. 10 Comparison between the stiffness in compression and tension experimentally measured and obtained by the model

are modelled. The stiffness of the epoxy joints used at the extremity of the beam is modelled by a torsion spring and the values are obtained by FE models realised from SEM observations.

- Even though we used a basic approach by taking the approximate values of the distance between the epoxy joints measured and the very simple junction model by FE, the stiffness in compression of entangled cross-linked fibres obtained fit well with that obtained from experimental data. So the model developed in this work seems to account for the physical phenomena.
- Effects of the junction stiffness and of the distance between them are studied in this work. As expected, the lower the inter-distance, the higher the stiffness. From the theoretical distance of an isotropic 3D assembly of fibres, the best stiffness can be determined. As the studied materials have all the same density, the highest stiffness is obtained in the case of carbon fibres.
- Irrespective of the nature of the fibres used, the material presents a higher stiffness in tension than in compression due to additional rigidity of the quasi vertical fibres, while in compression they buckle quickly [5]. With the help of the developed model, this additional rigidity due to the quasi-vertical fibres is determined by taking into account the fibres working in tension between the vertical and an angle θ_0 of 15°. Model values are a fairly good match with the experiments, so the concept according to which only a few fibres work in tension seems pertinent.

Acknowledgments Financial support for this work was obtained thanks to funding provided by the ANR (Agence National pour la Recherche) on the MANSART project.

References

1. Steeves, C.A., Fleck, N.A.: Material selection in sandwich beam construction. Scr. Mater. **50**, 1335–1339 (2004)
2. Allen, H.G.: Analysis and Design of Structural Sandwich Panels. Pergamon Press, Oxford (1969)
3. Zenkert, D.: The Handbook of Sandwich Construction. Chameleon Press Ltd, London (1997)
4. Vinson J.R.: The Behaviour of Sandwich Structures of Isotropic and Composite Materials. Technomic Publishing Co (1999)
5. Mezeix L., Poquillon P., Bouvet C.: Entangled cross-linked fibres for an application as core material for sandwich structures: part I: experimental investigation. Compos. Struct. (2010)
6. Golosnoy, I.O., Cockburn, A., Clyne, T.W.: Optimisation of metallic fibre network materials for compact heat exchangers. Adv. Eng. Mater. **10**(3), 210–218 (2008)
7. Zhang, B.M., Zhao, S.Y., He, X.D.: Experimental and theoretical studies on high-temperature thermal properties of fibrous insulation. J. Quant. Spectrosc. Radiat. Transf. **109**(7), 1309–1324 (2008)
8. Markaki, A.E., Clyne, T.W.: Mechanics of thin ultra-light stainless steel sandwich sheet material: part I. Stiffness. Acta Mater. **51**(5), 1341–1350 (2003)
9. Markaki, A.E., Clyne, T.W.: Mechanics of thin ultra-light stainless steel sandwich sheet material: part II. Resistance to delamination. Acta Mater. **51**(5), 1351–1375 (2003)
10. Dean J. et al.: Energy absorption during projectile perforation of lightweight sandwich panels with metallic fibre cores. International Conference of Sandwich Structure 8th (ICSS8), Porto, 6–8 May 2008
11. Masse, J.P., Bréchet, Y., Salvo, L., Bouaziz, O.: Mechanical Behavior of Non Sintered and Sintered Steel Wood. Material Research Society, Hong Kong (2008)
12. Markaki, A.E., Clyne, T.W.: Magneto-mechanical actuation of bonded ferromagnetic fibre arrays. Acta Mater. **53**, 877–889 (2005)
13. Gustavsson R.: Patent WO 98/01295, 15th January, AB Volvo, (1998)

14. Mezeix, L., Bouvet, C., Julitte, H., Poquillon, P.: Mechanical behaviour of entangled fibers and entangled cross-linked fibers during compression. J. Mater. Sci. **44**(14), 3652–3661 (2009)
15. Shahdin, A., Mezeix, L., Bouvet, C., Morlier, J., Gourinat, Y.: Fabrication and mechanical testing of glass fiber entangled sandwich beams: a comparison with honeycomb and foam sandwich beams. Compos. Struct. **90**(4), 404–412 (2009)
16. Shahdin, A., Mezeix, L., Bouvet, C., Morlier, J., Gourinat, Y.: Monitoring the effects of impact damages on modal parameters in carbon fiber entangled sandwich beams. Eng. Struct. **31**(12), 2833–2841 (2009)
17. Gibson, L.J., Ashby, M.F.: Cellular Solids, Structure and Properties, 2nd edn. Cambridge University Press, Cambridge (1997)
18. Zhou, D., Stronge, W.J.: Mechanical properties of fibrous core sandwich panels. Int. J. Mech. Sci. **47**(4–5), 775–798 (2005)
19. Ducheyne, P., Aernoudt, E., De Meester, P.: The mechanical behaviour of porous austenitic stainless steel fibre structures. J. Mater. Sci. **13**, 2650–2658 (1978)
20. Delannay, F.: Elastic model of an entangled network of interconnected fibres accounting for negative Poisson ratio behaviour and random triangulation. Int. J. Solids Struct. **42**(8), 2265–2285 (2005)
21. Underwood, E.E.: Quantitative Stereology. Addison Wesley Publishing Company, Reading (1970)
22. Toll, S.: Packing mechanics of fiber reinforcements. Polym. Eng. Sci. **38**, 1337–1350 (1998)
23. Dodson, C.T.J.: Fibre crowding, fiber contacts and fiber flocculation. Tappi J. **79**(9), 211–216 (1996)
24. Phillipse, A.P.: The random contact equation and its implications for (colloidal) rods in packings, suspensions, and anisotropic powders. Langmuir **12**(5), 1127–1133 (1996)